

Beta-delayed-neutron studies of $^{135,136}\text{Sb}$ and ^{140}I performed with trapped ions

B. S. Alan,^{1,2,*} S. A. Caldwell,^{3,4} N. D. Scielzo,¹ A. Czeszumaska,² J. A. Clark,^{4,5}
G. Savard,^{4,3} A. Aprahamian,⁶ M. T. Burkey,^{3,4} C. J. Chiara,^{4,7} J. Harker,^{4,7} A. F. Levand,⁴
S. T. Marley,^{8,6} G. E. Morgan,^{5,4} J. M. Munson,² E. B. Norman,² A. Nystrom,^{6,4} R. Orford,^{9,4}
S. W. Padgett,¹ A. Pérez Galván,^{4,10} K. S. Sharma,⁵ K. Siegl,⁶ and S. Y. Strauss⁶

¹Lawrence Livermore National Laboratory, Livermore, California 94550, USA

²Department of Nuclear Engineering, University of California, Berkeley, California 94720, USA

³Department of Physics, University of Chicago, Chicago, Illinois 60637, USA

⁴Physics Division, Argonne National Laboratory, Lemont, Illinois 60439, USA

⁵Department of Physics and Astronomy, University of Manitoba, Winnipeg, Manitoba R3T 2N2, Canada

⁶Department of Physics, University of Notre Dame, Notre Dame, Indiana 46556, USA

⁷Department of Chemistry and Biochemistry, University of Maryland, College Park, Maryland 20742, USA

⁸Department of Physics, Louisiana State University, Baton Rouge, Louisiana 70803, USA

⁹Department of Physics, McGill University, Montréal, Québec H3A 2T8, Canada

¹⁰Vertex Pharmaceuticals, San Diego, California 92121, USA

(Dated: November 1, 2021)

Beta-delayed-neutron (βn) spectroscopy was performed using the Beta-decay Paul Trap and an array of radiation detectors. The βn branching ratios and energy spectra for $^{135,136}\text{Sb}$ and ^{140}I were obtained by measuring the time of flight of recoil ions emerging from the trapped ion cloud. These nuclei are located at the edge of an isotopic region identified as having βn branching ratios that impact the r -process abundance pattern around the $A\sim 130$ peak. For $^{135,136}\text{Sb}$ and ^{140}I , βn branching ratios of 14.6(11)%, 17.6(28)%, and 7.6(28)% were determined, respectively. The βn energy spectra obtained for ^{135}Sb and ^{140}I are compared with results from direct neutron measurements, and the βn energy spectrum for ^{136}Sb has been measured for the first time.

I. INTRODUCTION

Beta-delayed-neutron (βn) emission is a process that can occur for neutron-rich nuclei sufficiently far from stability. In this process, a precursor nucleus undergoes β^- decay to a highly excited state in the daughter nucleus above the neutron-separation energy that emits a neutron. The properties of βn -emitting nuclei are important in various areas of basic and applied sciences, including nuclear astrophysics, nuclear energy, and nuclear structure.

The astrophysical rapid neutron-capture process (r process) is believed to be responsible for the production of roughly half of the elements heavier than iron [1, 2]. In the r process, neutron-rich nuclei far from stability are produced through repeated neutron-capture reactions, and βn emission during the eventual decay back to stability impacts the final isotopic abundance pattern. Different astrophysical environments, such as core-collapse supernovae [3, 4] and neutron-star mergers [5, 6], have been investigated as possible r -process sites by comparing theoretical models with observation. These models require high-quality nuclear data, such as nuclear masses, β -decay and neutron-capture rates, and βn -emission probabilities, for the thousands of isotopes along the nucleosynthesis pathway and populated during the decay back to stability. Much of this information still remains unknown, given the experimental challenges of accessing nuclei far from stability.

Beta-delayed-neutron emission also plays a key role in the control and safety of nuclear reactors. Both the branching ratios and energy spectra are required for reactor kinetics calculations and safety studies [7, 8]. Higher-quality nuclear data would allow for the βn yield and energy spectrum to be calculated for individual contributing isotopes, making it possible to accurately model any fuel-cycle concept, actinide mix, or irradiation history.

In addition, the information obtained in βn measurements helps to provide a better understanding of the nuclear structure of neutron-rich nuclei [9–12]. For example, measuring the βn -emission probability can be used to deduce the β -strength function above the neutron-separation energy of the daughter nucleus [13, 14]. Beta-delayed-neutron studies also help to constrain nuclear-structure calculations [15] and empirical models [16] that predict the decay properties of nuclei for which no data exist.

In this work, the Beta-decay Paul Trap (BPT) [17–19], a linear radiofrequency quadrupole ion trap with an open geometry, was utilized to study the βn branching ratios and energy spectra of a number of βn -emitting nuclei, which were produced with the Californium Rare Isotope Breeder Upgrade (CARIBU) facility [20] at Argonne National Laboratory. The results for $^{137,138}\text{I}$ and $^{144,145}\text{Cs}$ are discussed in Ref. [21], and the results for the more neutron-rich isotopes, $^{135,136}\text{Sb}$ and ^{140}I , are discussed here. Recent sensitivity studies performed by Mumpower *et al.* [22] indicate that the latter three nuclei are situated at the edge of a region in the nuclear chart where the βn branching ratios significantly impact the final r -process abundance pattern around the $A\sim 130$

* alan2@llnl.gov

peak.

II. EXPERIMENTAL METHODS

In the present work, the challenges associated with direct neutron detection are circumvented by instead studying the nuclear recoil from β decay. Radioactive ions are suspended in vacuum as a $\sim 1\text{-mm}^3$ cloud at the center of the BPT. When a trapped ion undergoes β decay, the recoil ion and emitted radiation emerge from the cloud with negligible scattering, allowing for their properties to be measured with radiation detectors arranged around the BPT as shown in Fig. 1. Two plastic-scintillator ΔE - E telescopes, two microchannel-plate (MCP) detectors, and two high-purity germanium (HPGe) detectors are used to measure β particles, recoil ions, and γ rays, respectively.

Beta-delayed-neutron spectroscopy is performed by recording the time of flight (TOF) of the recoil ions, which is determined from the time difference between the β particle hitting a ΔE detector and the recoil ion hitting an MCP detector. Due to the additional momentum imparted by the neutron, ions from βn emission have shorter TOFs than those from β decay without neutron emission. The recoil-ion momentum can be reconstructed from the TOF and the distance the ion travels to the MCP surface. The neutron energy may then be obtained through conservation of energy and momentum. The resulting neutron-energy spectrum can be determined down to 100 keV; at lower energies, TOF cannot be used to identify βn events because the corresponding recoil ions have energies comparable to those from β decays without neutron emission. In this section, the ion production, transport, and confinement, as well as the detection of the decay particles are discussed.

A. Beam delivery at CARIBU

At CARIBU, fission fragments from a $\sim 100\text{-mCi}$ ^{252}Cf source were thermalized in a large helium-filled gas catcher [20], extracted primarily as 1^+ ions, transported through an isobar separator [23], and delivered to a radiofrequency-quadrupole buncher containing a small amount of helium gas to accumulate, cool, and bunch the beam. The isobar separator had a mass resolution of $M/\Delta M \approx 14000$, which allowed for some suppression of isobars one neutron away from the desired species and essentially complete removal of isobars more than one neutron away.

The optimal isobar-separator settings were selected by monitoring the distribution of isotopes present in the beam during tuning. The beam composition was characterized by using the two HPGe detectors surrounding the BPT and by performing mass scans with the Canadian Penning Trap (CPT) mass spectrometer [24, 25]. The ion bunches were injected into the BPT at time inter-

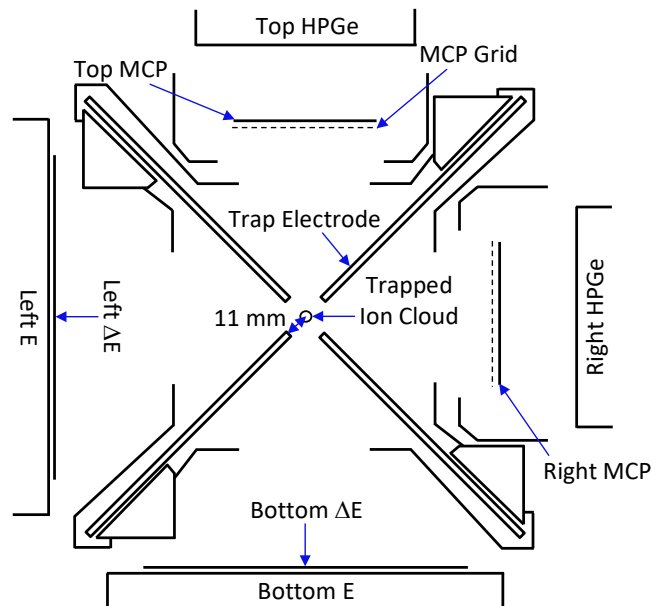


FIG. 1. (Color online) Cross-sectional view of the BPT and detectors used in the experiment (not to scale); the beam axis points perpendicularly into the plane. The detectors are labeled by their orientation relative to the beam direction at the center of the trap. Two plastic ΔE - E telescopes, two MCP detectors, and two HPGe detectors were used to measure β particles, recoil ions, and γ rays, respectively. Four sets of electrode plates were used to confine ions in the trap. Each plate came within 11 mm of the center of the BPT.

vals of t_{int} and accumulated over a length of time t_{meas} , after which the ions were ejected from the trap to measure backgrounds over a time period t_{bgd} ; this cycle was repeated throughout the entire run. The values of t_{int} , t_{meas} , and t_{bgd} used for each isotope are given in Table I and were chosen based on the radioactive half-life of the isotope being studied and the distribution of isobaric contaminants present during the measurement. The total measurement times and average beam rates are also shown in Table I.

B. Trapping with the BPT

Ion confinement was achieved by applying direct-current (DC) and time-varying, sinusoidal radiofrequency (RF) voltages to four sets of electrode plates extending to within 11 mm from the center of the trap as shown in Fig. 1. The DC voltages were used to produce a harmonic confining potential with a $\sim 5\text{-V}$ electrostatic valley in the axial direction, and the RF voltages, with a peak-to-peak amplitude of about 200 V and a frequency of 310 kHz, were used to confine ions in the radial direction. Higher harmonics at 620 and 930 kHz were observed with amplitudes less than 10% of the amplitude of the primary frequency. The trapped ions were thermalized

TABLE I. The measurement time, average beam rate, and trapping-cycle information (t_{int} , t_{meas} , t_{bkgd}) for the measurements. During each measurement cycle, ion bunches were injected into the BPT at time intervals of t_{int} , accumulated over a length of time t_{meas} , then ejected from the BPT for a background measurement lasting t_{bkgd} .

Isotope	Half-life (s)	Measurement time (h)	Average beam rate (ions/s)	t_{int} (s)	t_{meas} (s)	t_{bkgd} (s)
^{135}Sb	1.679(15) [26]	45.7	50	1.0	19.9	10.1
^{136}Sb	0.923(14) [27]	60.7	5	0.6	8.9	4.9
^{140}I	0.86(4) [28]	35.3	5	0.6	8.3	4.3

in $\sim 5 \times 10^{-5}$ Torr of helium gas.

Following β decay, the charge state of the recoil ion is typically 2^+ ; however, higher charge states can arise due to processes such as electron shakeoff, Auger-electron emission, and internal conversion. The stability conditions for the BPT, determined from the Mathieu equations [29], were chosen so that the decay daughters, which all have charge states higher than 1^+ , were not confined in the trap.

C. Particle detection

Two plastic-scintillator ΔE - E telescopes were used for β spectroscopy. The ΔE detector was a 1-mm-thick, 10.6-cm-diameter disk that had a nearly 100% intrinsic detection efficiency for β particles and only a $\sim 1\%$ intrinsic detection efficiency for γ rays and neutrons. The ΔE detectors were placed ~ 105 mm from the center of the BPT and each covered a solid angle of 5% of 4π . The E detectors were 10.2-cm-thick, 13.3-cm-diameter disks located immediately behind the ΔE detectors that were capable of stopping the β particles. Each ΔE - E telescope was contained in its own vacuum chamber (held below 10^{-3} Torr) and separated from the BPT vacuum by a 10- μm -thick aluminized-Kapton window. The Left and Bottom ΔE detectors had β -energy thresholds of 76(24) keV and 62(30) keV, respectively, and a neutron detection threshold of 370(70) keV [21].

Two 50.3×50.3 mm² resistive-anode Chevron MCP detectors [30] with 1-ns timing resolution and sub-mm position sensitivity were used for recoil-ion detection. The front face of each detector was biased to approximately -2.5 kV to accelerate incoming ions and thereby provide a more uniform detection efficiency. Each detector was placed 4.5 mm behind a grounded 89%-transmission grid to help shield the detector from the RF fields of the BPT and to prevent the recoil-ion trajectories from being affected by the MCP bias voltage until they passed through the grid. The hit locations of the ions were reconstructed from the relative amounts of charge collected at the four corners of the anode [31]. The central 46×46 mm² region of each MCP detector had the best position resolution and was taken to be the fiducial area in the data analysis. Each detector was located 53.0(5) mm away from the trap center and subtended a solid-angle of 5% of 4π .

The intrinsic efficiencies of the MCP detectors were determined to be 33.3(15)% and 29.3(14)% for the Right and Top detectors, respectively, from a detailed study of the decays of trapped ^{134}Sb ions held in the BPT [32]. The ion detection efficiencies also had to be corrected for additional loss of MCP pulses to electronic thresholds [21, 33]. For the Right MCP detector, this was a $<3\%$ correction. However, the Top MCP detector had a lower gain, resulting in a correction that ranged between ~ 5 – 30% (depending on the impact energy of the ions) and showed some spatial dependence.

Two coaxial single-crystal p-type HPGe detectors were used to detect γ rays. The detectors, which had relative efficiencies of 80% and 140%, were located within 10 cm of the trapped-ion cloud behind the Right and Top MCP detectors, respectively. Standard γ -ray point sources (^{60}Co , ^{133}Ba , ^{137}Cs , ^{152}Eu) with activities determined to within 1.5–2.5% (at 1σ) were used to calibrate the photopeak detection efficiencies.

The data-acquisition system was triggered on a signal from any detector. A 22- μs coincidence window was then opened, during which the amplitude and timing of each detected event was recorded along with the phase of the BPT RF voltage. The TOF for recoil ions was determined with a timing resolution of 3 ns FWHM. The nonparalyzable deadtime per event was 142 μs .

III. ANALYSIS AND RESULTS

The TOF of the recoil ions was determined from ΔE -MCP detector coincidences and used to distinguish βn decays from β decays without neutron emission. The TOF spectra measured for $^{135,136}\text{Sb}$ and ^{140}I are shown in Fig. 2. The βn events have TOFs primarily between 200 and 2000 ns, and β -decay events without neutron emission have longer TOFs. A peak at 0 ns arose from β -particle events in the ΔE detector that were in coincidence with a γ ray or scattered β particle triggering the MCP detector.

The βn energy spectra and branching ratios determined from these TOF spectra are discussed in this section. The Monte Carlo simulations of the decays and experimental setup needed to analyze the data are introduced first.

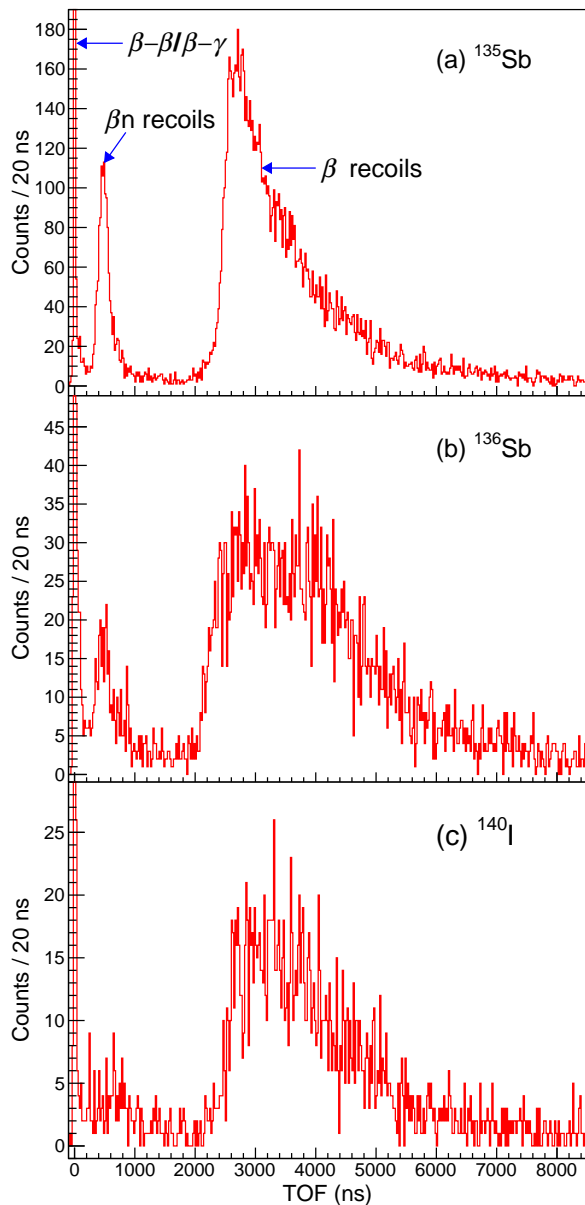


FIG. 2. (Color online) TOF spectra for (a) ^{135}Sb , (b) ^{136}Sb , and (c) ^{140}I . Events between 200 and 2000 ns are primarily due to recoil ions from βn decay, and events above 2000 ns are primarily due to recoil ions from β decay without neutron emission. The peak at 0 ns is due to coincidences where a β particle hit a ΔE detector and a γ ray or scattered β particle triggered an MCP detector.

A. Monte Carlo simulations

The β -decay kinematics were generated using simulation code originally developed in Ref. [34] and later adapted for βn decay [17, 32, 35]. For each β -decay transition, a distribution of β and ν momenta was generated, assuming an allowed β -spectrum shape. For excited states, the subsequent deexcitation to the ground state

by the emission of γ rays, conversion electrons (CEs), and neutrons was also included. The resulting nuclear recoil was determined from the momentum imparted from each of these decay particles. For βn emission, the transitions were assumed to be allowed Gamow-Teller and assigned a β - ν angular correlation, $a_{\beta\nu}$, of $-1/3$. For transitions to states below the neutron-separation energy, an approximation was made that for a given isotope, all the $a_{\beta\nu}$ were fixed to a single value, which was determined from the measured β -ion coincidences using an approach described in detail in Ref. [35]. For ^{135}Sb and ^{140}I , this value of $a_{\beta\nu}$ was $+0.23$ and -0.42 , respectively. For ^{136}Sb , the presence of trapped ^{136}Te ions complicated the analysis of the recoil ions and a value for $a_{\beta\nu}$ could not be obtained.

The β decays were spatially distributed with a 1-mm-FWHM Gaussian distribution in three dimensions, corresponding to the measured ion-cloud extent [32]. The emitted β particles, γ rays, CEs, and neutrons were propagated using GEometry ANd Tracking 4 (GEANT4) [36, 37] version 4.10.0.p01 to model the scattering and energy loss of the particles within the apparatus. The energies deposited in the ΔE , E , and HPGe detectors were recorded, and the electronic thresholds of the ΔE detectors were taken into account. Recoil ions of various charge states were propagated through the time-varying electric fields of the BPT using the SIMION 8.1 [38] ion-optics code. The average charge states following the decay of $^{135,136}\text{Sb}$ and ^{140}I were determined to be 2.20, 2.51, and 2.16, respectively [35], from the RF-phase dependence of the measured β -ion coincidence rate using the approaches described in Ref. [32]. For ions that struck an MCP detector, a threshold cut was applied [21] and the TOF, energy, velocity, and position at impact were recorded.

The efficiencies for detecting β particles and β -ion coincidences were determined using these simulations. Fig. 3 shows the β -ion-coincidence detection efficiency as a function of neutron energy for ^{135}Sb , with the product of the corresponding detector solid angles and MCP-detector intrinsic efficiency divided out. At the highest neutron energies, the coincidence-detection efficiency drops rapidly because of the limited energy available for the leptons, which results in fewer β particles having energies above the ΔE detector thresholds. However, β decays that populate highly-excited states are largely suppressed because of phase-space considerations. The two 180° combinations (Left-Right and Bottom-Top) have higher efficiencies than the two 90° combinations (Left-Top and Bottom-Right) primarily because of neutron-ion coincidences, which are present because the neutron and recoil ion are emitted with momenta nearly 180° apart and therefore strike back-to-back detectors. The β -ion-coincidence detection-efficiency curves for ^{136}Sb and ^{140}I have similar features.

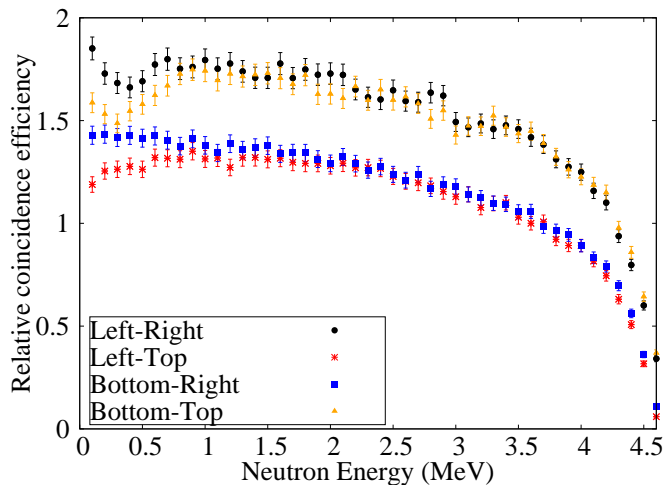


FIG. 3. (Color online) The β -ion-coincidence detection efficiency for each ΔE -MCP detector pair as a function of neutron energy for ^{135}Sb ; the product of the corresponding detector solid angles and MCP-detector intrinsic efficiency has been divided out. The two 180° combinations (Left-Right and Bottom-Top) have higher efficiencies than the two 90° combinations (Left-Top and Bottom-Right) primarily because of additional events from neutron-ion coincidences. At the highest neutron energies, the coincidence detection efficiency drops rapidly because of the limited energy available for the leptons; however, few β decays are expected to yield neutrons at these energies because of phase-space considerations. The β -ion-coincidence detection-efficiency curves for ^{136}Sb and ^{140}I have similar features.

B. Neutron energy spectra

The neutron energy was obtained by assuming the recoil ion and neutron had equal and opposite momenta. The momentum was approximated from the recoil-ion TOF and hit position on the MCP surface; the distance traveled by the recoil ion was approximated as a straight path from the trap center to the MCP grid, and effects due to the acceleration of the ion between the grid and the MCP surface were corrected for analytically. Background events were subtracted from the resulting spectrum, after which the neutron energy was adjusted to account for the contribution to the recoil-ion momentum from lepton emission. The spectrum was then scaled by the β -ion coincidence efficiency. Each of these data analysis steps is explained below.

The background from accidental coincidences was determined from the TOF region between $15\text{--}20\ \mu\text{s}$, which both data and simulation indicated had no true β -ion coincidences. This subtraction resulted in a 3–9% correction, depending on the isotope.

After accounting for accidental coincidences, counts remained in the $50\text{--}200\text{-ns}$ time window where no β -ion coincidences from trapped ions were expected. These counts were present both while the BPT was trapping ions and while the BPT was held empty following ejection

of the trapped ions and were likely due to radioactivity that accumulated on the BPT and detector surfaces during data collection. The TOF distribution of these events was most pronounced between $50\text{--}200\ \text{ns}$ and decreased with increasing TOF, extending into the βn TOF region. The shape of this background, when converted into a neutron-energy distribution, closely resembled an exponential function. The subtraction of this background was performed by normalizing this exponential function to match the number of counts between $50\text{--}200\ \text{ns}$ collected when the BPT was trapping ions. This resulted in a 15–30% correction to the total number of observed βn decays, depending on the isotope being analyzed.

During data collection, isobaric contaminants one neutron away from the isotope of interest were suppressed but not completely removed. For $^{135,136}\text{Sb}$ and ^{140}I , the more neutron-rich isobar ($^{135,136}\text{Sn}$ and ^{140}Te , respectively) is a βn emitter, but has a ^{252}Cf -fission yield a couple orders of magnitude lower than the isotope of interest, making its contribution to the total number of βn decays in the BPT negligible. For ^{135}Sb and ^{140}I , the more proton-rich isobar (^{135}Te and ^{140}Xe , respectively) does not decay by βn emission and therefore cannot contribute βn events. For ^{136}Sb , the more proton-rich isobar, ^{136}Te , has a βn branching ratio roughly ten times smaller than that of ^{136}Sb , but a fission yield 30 times larger. The suppression of ^{136}Te by the isobar separator, together with the measurement cycle favoring the shorter-lived species, resulted in an average trapped-ion activity with about 15% more ^{136}Sb than ^{136}Te . The ^{136}Te contribution to the total number of βn coincidences was determined to be 5% based on the ratio of the ^{136}Sb and ^{136}Te activities, after accounting for the βn branching ratios and the fraction of neutrons with energies above the 100-keV neutron threshold (estimated to be $0.6(2)$ for ^{136}Te from the neutron-energy spectrum in Ref. [39] and determined in Sec. III C to be $0.89(6)$ for ^{136}Sb).

The neutron energy determined solely from the recoil momentum was adjusted to account for the momentum imparted to the recoil ion from lepton emission. For the β -ion coincidences measured by detectors 180° apart, the neutron energy tended to be overestimated because the β particle was emitted in approximately the same direction as the neutron and therefore contributed to the momentum of the nuclear recoil. Simulations showed that neglecting the leptons resulted in an overestimation of the inferred neutron energy of 25–30% at 100 keV, which steadily decreased to 10%, 7%, and $<4\%$ at neutron energies of 500 keV, 1000 keV, and above 2000 keV, respectively. For the β -ion coincidences measured by detectors 90° apart, the overestimation was only 1–2% for all neutron energies. For ^{136}Sb and ^{140}I , the neutron emission was assumed to directly populate the ground state, as there is currently no data indicating that excited states are populated. For ^{135}Sb , however, decays to the ground state as well as the first, second, and third excited states (populated with probabilities of 62%, 21%, 11%, and 6%, respectively [40]) were taken into account,

and the inclusion of the excited states led to a 1% shift in the inferred neutron energy.

For each isotope, the neutron-energy spectrum obtained for each ΔE -MCP detector pair was corrected by the corresponding neutron-energy-dependent β -ion coincidence efficiency. The results summed together for the four ΔE -MCP detector pairs are shown in Fig. 4 for $^{135,136}\text{Sb}$ and ^{140}I . For ^{136}Sb , the contribution from ^{136}Te isobaric contamination was removed by subtracting the ^{136}Te neutron-energy spectrum measured in Ref. [39], which was scaled by the activity and β_n branching ratio and broadened to account for the experimental energy resolution. The neutron-energy resolution in the present work was primarily determined by the spatial distribution of the ion cloud and the spread in recoil momentum resulting from the lepton emission. Simulations indicated that the FWHM energy resolution was 60% at a neutron energy of 100 keV and steadily decreased to 25%, 15%, and 9% at 500 keV, 1000 keV, and above 2000 keV, respectively. The neutron energy spectrum was determined down to ~ 100 keV; below this energy, the recoil momentum imparted from the emission of the leptons and any accompanying γ rays was comparable to the momentum imparted from neutron emission.

For ^{135}Sb and ^{140}I , the neutron-energy spectra are compared with direct neutron measurements by Kratz *et al.* [14] and Shalev and Rudstam [41], respectively. For ^{136}Sb , no previous measurement of the energy spectrum has been made. In the experiment by Kratz *et al.*, β_n precursors were produced through neutron-induced fission of ^{235}U at the Mainz TRIGA reactor, and two ^3He ionization chambers, with energy resolutions of ~ 12 keV for thermal neutrons and ~ 20 keV for 1-MeV neutrons, were used to measure neutron energies. In the experiment by Shalev and Rudstam, β_n precursors were produced at the OSIRIS isotope-separator on-line facility. Neutron energies were measured with a neutron spectrometer that consisted of a cylindrical gridded ionization chamber filled with a ^3He -argon gas mixture. The results obtained with the BPT for ^{135}Sb and ^{140}I have neutron-energy spectra and energy thresholds that are similar to the direct measurements. For ^{135}Sb , the peaks in the spectrum obtained here are not as sharp because of the wider energy resolution; it also appears that there is a 4% energy shift in some of the features. The energy calibration in the present work depended primarily on the distance between the ion cloud and MCP detectors — this distance was determined with a fractional precision of 1%, with consistent values obtained from both the measurement of the location of the trap electrodes and detectors and an analysis of the recoil-ion TOF spectra [32]. This results in a 2% uncertainty in the neutron energy. An additional 1% uncertainty in the neutron energy was attributed to the energy shift applied to account for the lepton emission.

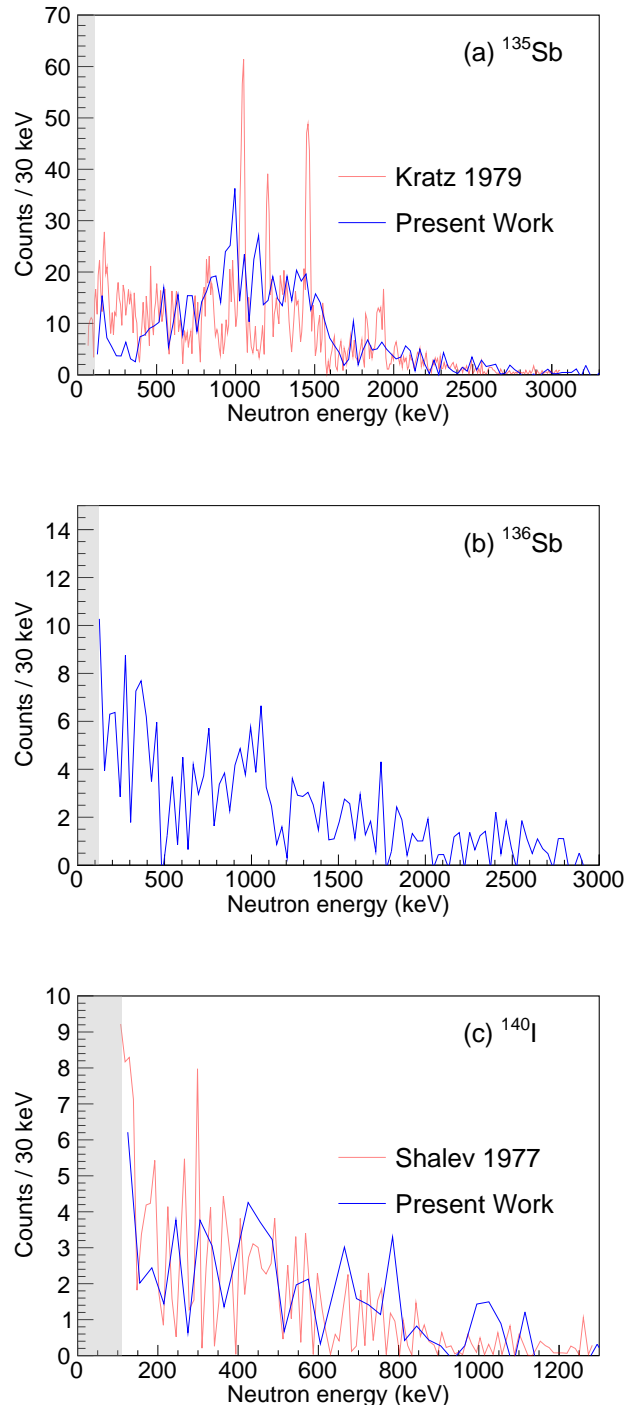


FIG. 4. (Color online) Neutron energy spectra for (a) ^{135}Sb , (b) ^{136}Sb , and (c) ^{140}I compared with results from Kratz *et al.* [14] and Shalev and Rudstam [41]. The y-axis label refers to the present work, where each data point corresponds to a 30-keV-wide bin. For the ^{135}Sb spectrum measured by Kratz *et al.* and the ^{140}I spectrum measured by Shalev and Rudstam, the data points correspond to ~ 8 -keV-wide and ~ 10.75 -keV-wide bins, respectively. In the gray region below ~ 100 keV, no neutron-energy information was obtained in the present work because the TOF of recoils from β_n emission could not be distinguished from those from β decay without neutron emission.

C. βn branching ratios

The βn branching ratios were obtained by comparing the number of detected β -ion coincidences corresponding to decays that emitted a neutron with energy above 100 keV, $n_{\beta R}$, to the number of detected β particles, n_{β} , through the relation

$$P_n = \frac{n_{\beta R}/(\epsilon_{\beta R} \cdot f)}{n_{\beta}/\epsilon_{\beta}}, \quad (1)$$

where $\epsilon_{\beta R}$ is the efficiency for detecting the β -ion coincidences and ϵ_{β} is the β -particle detection efficiency. The ratio $\epsilon_{\beta}/\epsilon_{\beta R}$ was determined from simulations with an uncertainty of 5%. The fraction f of the βn spectrum with neutron energies above 100 keV was obtained by assuming the neutron spectrum below threshold has the same intensity as the 100 keV above threshold, as there is currently no information on the neutron spectra at these low energies. This assumption yielded values of 0.95(3), 0.89(6), and 0.83(9) for ^{135}Sb , ^{136}Sb and ^{140}I , respectively, and an uncertainty of half the difference from unity was assigned. Given that there do not appear to be pronounced features in the low-energy portions of these spectra, it is unlikely that there is large peak below 100 keV that would skew these estimates. To determine n_{β} , the ΔE triggers originating from the trapped species of interest were isolated from those due to decays of isobaric contaminants and other backgrounds. This was accomplished by comparing the data to a model that takes into account the buildup and decay of the different species in the BPT over the course of the trapping cycle, while enforcing the decay-feeding relationships between the different populations [42]. The results for n_{β} were obtained with 5% precision.

For ^{135}Sb and ^{140}I , the βn branching ratio was also obtained directly from the recoil-ion TOF spectrum by comparing $n_{\beta R}$ to the number of β -ion coincidences observed for decays without neutron emission, $n_{\beta r}$, using

$$P_n = \frac{n_{\beta R}/(\epsilon_{\beta R} \cdot f)}{n_{\beta R}/(\epsilon_{\beta R} \cdot f) + n_{\beta r}/\epsilon_{\beta r}}, \quad (2)$$

where $\epsilon_{\beta r}$ is the efficiency for detecting β -ion coincidences without neutron emission and was determined in Ref. [35]. The $n_{\beta r}$ results were obtained by selecting the events in the TOF region where β decays without neutron emission are expected and subtracting the contribution from isobaric contaminants (when present) and accidental coincidences. For ^{135}Sb and ^{140}I , $n_{\beta r}$ was determined with 3% and 6% precision, respectively. The ratio $\epsilon_{\beta R}/\epsilon_{\beta r}$ had an uncertainty of 5%. For ^{136}Sb , the trapped ^{136}Te activity was substantial enough to make its subtraction from $n_{\beta r}$ challenging, and therefore, a reliable value for $n_{\beta r}$ could not be obtained.

The βn branching ratios were obtained from the weighted average of the results from the four ΔE -MCP

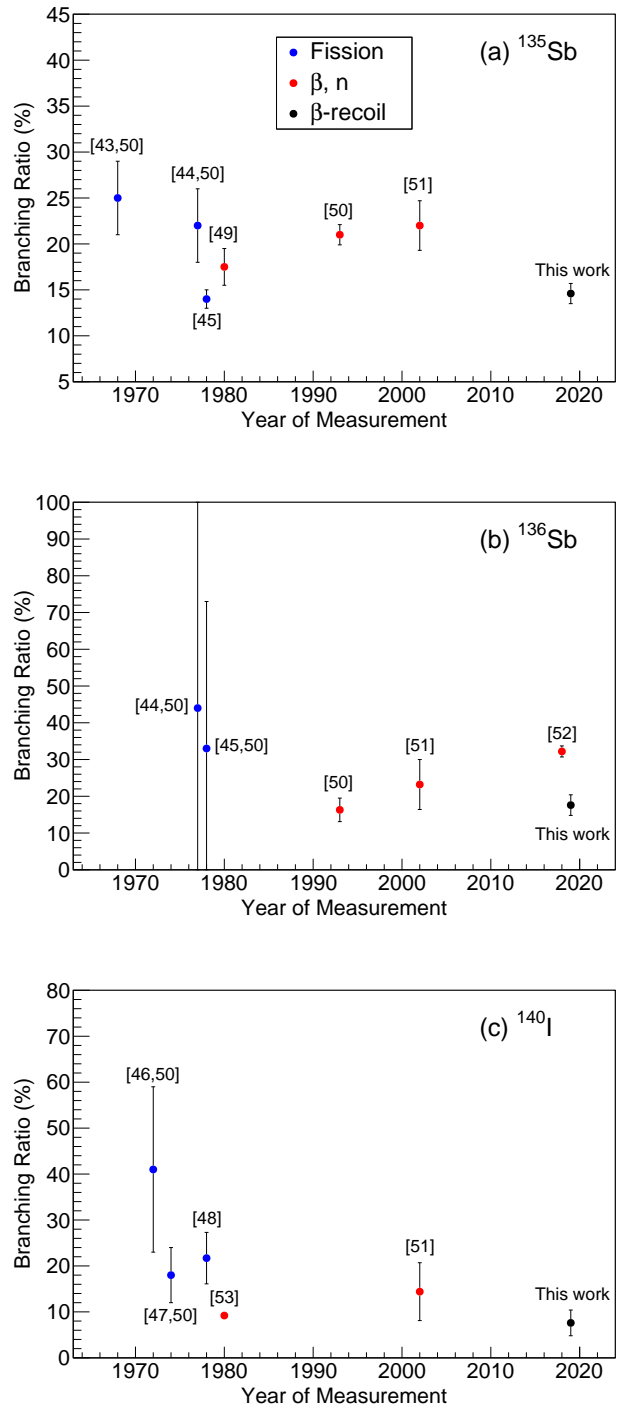


FIG. 5. (Color online) Beta-delayed-neutron branching ratios from the present work (values taken from Table II) compared with previous direct measurements for (a) ^{135}Sb , (b) ^{136}Sb , and (c) ^{140}I . The corresponding year, reference(s), and measurement technique are provided for each measurement. The label “fission” indicates that P_n was obtained from the fission yield and neutrons-per-fission of the isotope. “ β, n ” indicates that P_n was obtained by counting β particles and neutrons separately, usually with plastic scintillators and neutron detectors (e.g., BF_3 tubes, ^3He tubes), respectively, and “ β -recoil” refers to the present work.

TABLE II. Recommended βn branching ratios obtained in the present work. Uncertainties are divided into statistical and systematic.

Isotope	P_n (%)
^{135}Sb	14.6 ± 0.4 (stat) ± 1.0 (sys)
^{136}Sb	17.6 ± 1.0 (stat) ± 2.6 (sys)
^{140}I	7.6 ± 0.9 (stat) ± 2.6 (sys)

detector pairs. For ^{135}Sb and ^{140}I , P_n values of 14.6(16)% and 8.1(34)%, respectively, were determined from Eq. 1, and values of 14.6(11)% and 7.6(28)%, respectively, were determined from Eq. 2. For ^{136}Sb , Eq. 1 yielded a P_n of 17.6(28)%. In these approaches to determining P_n , the systematic uncertainty due to the β -particle detection efficiency largely cancels out. However, obtaining P_n directly from the recoil-ion TOF spectrum yields a smaller total uncertainty because the systematic uncertainties due to the MCP solid angles and intrinsic efficiencies also cancel out. Therefore, for ^{135}Sb and ^{140}I , the βn branching ratios obtained from the recoil-ion TOF spectrum are recommended; for ^{136}Sb , only the P_n value obtained from the comparison to detected β particles is available. In Table II, the recommended βn branching-ratio results are provided. These values are compared with results obtained from previous direct measurements in Fig. 5. In the direct measurements, P_n was determined either from the fission yield and neutrons-per-fission of the isotope [43–48], or by counting β particles and neutrons separately [49–53], usually with plastic scintillators and neutron detectors (e.g., BF_3 tubes, ^3He tubes), respectively. For each isotope, there is roughly a factor of two spread among the P_n results, despite the fact that in many cases, the quoted uncertainties are significantly smaller than these differences. These discrepancies are evident even when comparing measurements that used similar experimental techniques, underscoring the challenging nature of performing βn spectroscopy and indicating unforeseen systematic effects were likely responsible for these differences.

The P_n results for $^{135,136}\text{Sb}$ and ^{140}I were determined in an analogous manner to the results for $^{137,138}\text{I}$ and $^{144,145}\text{Cs}$ in Ref. [21]. In Ref. [21], the βn branching ratios were obtained by comparing the number of β -ion coincidences corresponding to βn decay to the β -decay activity, which was measured three different ways: (1) from the number of β particles detected by the ΔE detectors, (2) from the number of β -ion coincidences registered by the ΔE and MCP detectors, and (3) from the number of β - γ coincidences registered by the ΔE and HPGe detectors. These three independent measures gave consistent P_n results that were in excellent agreement with previous direct measurements. They also gave an opportunity to probe systematic effects and provided confidence that they were under control. In the present work, P_n was obtained using methods (1) and (2), with limited statistics for β -delayed γ -ray emission not allowing method

(3). For ^{135}Sb and ^{140}I , where P_n from methods (1) and (2) could be compared, consistent results were again obtained.

IV. SUMMARY AND CONCLUSIONS

Beta-delayed-neutron spectroscopy was performed using the BPT instrumented with two plastic-scintillator ΔE - E telescopes, two MCP detectors, and two HPGe detectors to measure β particles, recoil ions, and γ rays, respectively. Both the βn energy spectra and branching ratios were determined for the neutron-rich nuclei $^{135,136}\text{Sb}$ and ^{140}I . The βn energy spectrum for ^{136}Sb was measured for the first time, and the spectra for ^{135}Sb and ^{140}I were compared with results from direct neutron measurements by Kratz *et al.* [14] and Shalev and Rudstam [41], respectively. The βn energy spectra from the present work were similar in shape and had comparable energy thresholds to those obtained through direct neutron detection. The βn branching ratios were obtained by comparing the number of β -ion coincidences from βn decays to the number of detected β decays, which was determined from the number of β particles registered by the ΔE detector and, when possible, the number of β -ion coincidences. The latter approach to determining the number of detected β decays was preferred when available, as it resulted in smaller systematic uncertainties in P_n .

The neutron-energy spectra were obtained with β -ion-coincidence efficiencies of $\sim 0.5\%$, which is several orders of magnitude larger than the neutron-detection efficiencies achievable with the ^3He and gas-proportional detectors used for direct neutron spectroscopy. The ion-trap approach is therefore well suited for use at radioactive-beam facilities, where efficient techniques are desired to make the most of the delivered beam intensities. The βn branching ratios for ^{136}Sb and ^{140}I were determined with beam intensities of only 5 ions/s, and with improvements to the detector array, results could be obtained with beams of less than 1 ion/s.

Upgrades to the BPT setup are currently in development. Plans include increasing the β -recoil-coincidence detection efficiency using larger plastic scintillators and MCP detectors, and lowering the neutron energy threshold by further minimizing the impact of the electric fields on the trajectories of the recoil ions. The latter will be accomplished by bringing the electrodes closer to the center of the ion trap to allow for a lower-amplitude RF voltage to be applied, thus reducing the perturbation of the ion trajectories while the ions are in transit to the MCP detectors. Future experiments will also benefit from the increased intensities and purities of the beams delivered by the CARIBU facility [54, 55]; since these measurements were performed, the beam intensities have increased by an order of magnitude. These improvements will allow βn measurements to be performed for neutron-rich nuclei even further from stability, allowing access to many

of the isotopes that significantly impact r -process nucleosynthesis.

V. ACKNOWLEDGEMENTS

We acknowledge and appreciate the assistance of the ATLAS staff. This material is based upon work supported by the Department of Energy, National Nuclear

Security Administration, under Award Numbers DE-NA0000979 (NSSC), DE-AC52-07NA27344 (LLNL), and DE-NA0002135 (SSGF); Office of Nuclear Physics Contract DE-AC02-06CH11357 (ANL); NEUP Project Number 13-5485 (University of California); Grant DE-FG02-94ER40834 (University of Maryland); Louisiana State Board of Regents Research Competitiveness Subprogram LEQSF(2016-19)-RD-A-09; NSERC, Canada, under Application No. 216974; NSF contract PHY-1419765; and the Department of Homeland Security.

-
- [1] E. M. Burbidge, G. R. Burbidge, W. A. Fowler, and F. Hoyle, *Rev. Mod. Phys.* **29**, 547 (1957).
- [2] A. G. W. Cameron, *Publ. Astron. Soc. Pac.* **69**, 201 (1957).
- [3] B. S. Meyer, G. J. Mathews, W. M. Howard, S. E. Woosley, and R. D. Hoffman, *Astrophys. J.* **399**, 656 (1992).
- [4] K. Farouqi, K.-L. Kratz, B. Pfeiffer, T. Rauscher, F.-K. Thielemann, and J. W. Truran, *Astrophys. J.* **712**, 1359 (2010).
- [5] S. Goriely, A. Bauswein, and H.-T. Janka, *The Astrophys. J.* **738**, L32 (2011).
- [6] E. Pian, P. D’Avanzo, S. Benetti, M. Branchesi, E. Brocato, S. Campana, E. Cappellaro, S. Covino, V. D’Elia, J. P. U. Fynbo, *et al.*, *Nature* **551**, 67 (2017).
- [7] S. Das, *Prog. Nucl. Energy* **28**, 209 (1994).
- [8] A. D’Angelo, *Prog. Nucl. Energy* **41**, 1 (2002).
- [9] K.-L. Kratz, *Nucl. Phys. A* **417**, 447 (1984).
- [10] S. Raman, B. Fogelberg, J. A. Harvey, R. L. Macklin, P. H. Stelson, A. Schröder, and K.-L. Kratz, *Phys. Rev. C* **28**, 602 (1983).
- [11] J. H. Hamilton, P. G. Hansen, and E. F. Zganjar, *Rep. Prog. Phys.* **48**, 631 (1985).
- [12] J. A. Winger, S. V. Ilyushkin, K. P. Rykaczewski, C. J. Gross, J. C. Batchelder, C. Goodin, R. Grzywacz, J. H. Hamilton, A. Korgul, W. Królas, *et al.*, *Phys. Rev. Lett.* **102**, 142502 (2009).
- [13] A. C. Pappas and T. Sverdrup, *Nucl. Phys.* **A188**, 48 (1972).
- [14] K.-L. Kratz, W. Rudolph, H. Ohm, H. Franz, M. Zendel, G. Herrmann, S. G. Prussin, F. M. Nuh, A. A. Shihab-Eldin, D. R. Slaughter, W. Halverson, and H. V. Klapdor, *Nucl. Phys. A* **317**, 335 (1979).
- [15] T. Kawano, P. Möller, and W. B. Wilson, *Phys. Rev. C* **78**, 054601 (2008).
- [16] E. A. McCutchan, A. A. Sonzogni, T. D. Johnson, D. Abriola, M. Birch, and B. Singh, *Phys. Rev. C* **86**, 041305 (2012).
- [17] R. M. Yee, N. D. Scielzo, P. F. Bertone, F. Buchinger, S. Caldwell, J. A. Clark, C. M. Deibel, J. Fallis, J. P. Greene, S. Gulick, *et al.*, *Phys. Rev. Lett.* **110**, 092501 (2013).
- [18] N. D. Scielzo, G. Li, M. G. Sternberg, G. Savard, P. F. Bertone, F. Buchinger, S. Caldwell, J. A. Clark, J. Crawford, C. M. Deibel, *et al.*, *Nucl. Instrum. Methods Phys. Res. A* **681**, 94 (2012).
- [19] N. D. Scielzo, R. M. Yee, P. F. Bertone, F. Buchinger, S. A. Caldwell, J. A. Clark, A. Czeszumaska, C. M. Deibel, J. P. Greene, S. Gulick, *et al.*, *Nucl. Data Sheets* **120**, 70 (2014).
- [20] G. Savard, S. Baker, C. Davids, A. F. Levand, E. F. Moore, R. C. Pardo, R. Vondrasek, B. J. Zabransky, and G. Zinkann, *Nucl. Instrum. Methods Phys. Res. B* **266**, 4086 (2008).
- [21] A. Czeszumaska *et al.*, (in preparation).
- [22] M. R. Mumpower, R. Surman, G. C. McLaughlin, and A. Aprahamian, *Prog. Part. Nucl. Phys.* **86**, 86 (2016).
- [23] C. N. Davids and D. Peterson, *Nucl. Instrum. Methods Phys. Res. B* **266**, 4449 (2008).
- [24] G. Savard, R. C. Barber, D. Beeching, F. Buchinger, J. E. Crawford, S. Gulick, X. Feng, E. Hagberg, J. C. Hardy, V. T. Koslowsky, *et al.*, *Nucl. Phys. A* **626**, 353 (1997).
- [25] J. C. Wang, G. Savard, K. S. Sharma, J. A. Clark, Z. Zhou, A. F. Levand, C. Boudreau, F. Buchinger, J. E. Crawford, J. P. Greene, *et al.*, *Nucl. Phys. A* **746**, 651 (2004).
- [26] B. Singh, A. A. Rodionov, and Y. L. Khazov, *Nucl. Data Sheets* **109**, 517 (2008).
- [27] A. A. Sonzogni, *Nucl. Data Sheets* **95**, 837 (2002).
- [28] N. Nica, *Nucl. Data Sheets* **108**, 1287 (2007).
- [29] W. Paul, *Rev. Mod. Phys.* **62**, 531 (1990).
- [30] J. L. Wiza, *Nucl. Instrum. Methods* **162**, 587 (1979).
- [31] M. Lampton and C. W. Carlson, *Rev. Sci. Instrum.* **50**, 1093 (1979).
- [32] K. Siegl, N. D. Scielzo, A. Czeszumaska, J. A. Clark, G. Savard, A. Aprahamian, S. A. Caldwell, B. S. Alan, M. T. Burkey, C. J. Chiara, *et al.*, *Phys. Rev. C* **97**, 035504 (2018).
- [33] A. Czeszumaska, Ph.D. thesis, University of California, Berkeley, Department of Nuclear Engineering (2016).
- [34] N. D. Scielzo, S. J. Freedman, B. K. Fujikawa, and P. A. Vetter, *Phys. Rev. A* **68**, 022716 (2003).
- [35] J. M. Munson, K. Siegl, N. D. Scielzo, B. S. Alan, A. Czeszumaska, G. Savard, A. Aprahamian, S. A. Caldwell, C. J. Chiara, J. A. Clark, *et al.*, *Nucl. Instrum. Methods Phys. Res. A* **898**, 60 (2018).
- [36] S. Agostinelli, J. Allison, K. Amako, J. Apostolakis, H. Araujo, P. Arce, M. Asai, D. Axen, S. Banerjee, G. Barrand, *et al.*, *Nucl. Instrum. Methods Phys. Res. A* **506**, 250 (2003).
- [37] J. Allison, K. Amako, J. Apostolakis, H. Araujo, P. Arce Dubois, M. Asai, G. Barrand, R. Capra, S. Chauvie, R. Chytráček, *et al.*, *IEEE Trans. Nucl. Sci.* **53**, 270 (2006).
- [38] D. Manura and D. Dahl, *SIMION 8.0/8.1 User Manual (Scientific Instrument Services, Inc. Ringoes, NJ 08551)* (2008).

- [39] S. Shalev and G. Rudstam, Nucl. Phys. A **230**, 153 (1974).
- [40] P. Hoff, B. Ekström, and B. Fogelberg, Z. Phys. A **332**, 407 (1989).
- [41] S. Shalev and G. Rudstam, Nucl. Phys. A **275**, 76 (1977).
- [42] S. A. Caldwell, Ph.D. thesis, University of Chicago, Department of Physics (2015).
- [43] L. Tomlinson and M. H. Hurdus, J. Inorg. Nucl. Chem. **30**, 1649 (1968).
- [44] W. Rudolph, K.-L. Kratz, and G. Herrmann, J. Inorg. Nucl. Chem. **39**, 753 (1977).
- [45] J. Crançon, C. Ristori, H. Ohm, W. Rudolph, K.-L. Kratz, and M. Asghar, Z. Phys. A **287**, 45 (1978).
- [46] H.-D. Schüssler and G. Herrmann, Radiochim. Acta **18**, 123 (1972).
- [47] K.-L. Kratz and G. Herrmann, Nucl. Phys. A **229**, 179 (1974).
- [48] K.-L. Kratz, Radiochim. Acta **25**, 1 (1978).
- [49] E. Lund, P. Hoff, K. Aleklett, O. Glomset, and G. Rudstam, Z. Phys. A **294**, 233 (1980).
- [50] G. Rudstam, K. Aleklett, and L. Sihver, At. Data Nucl. Data Tables **53**, 1 (1993).
- [51] B. Pfeiffer, K.-L. Kratz, and P. Möller, Prog. Nucl. Energy **41**, 39 (2002).
- [52] R. Caballero-Folch, I. Dillmann, J. Agramunt, J. L. Taín, A. Algora, J. Äystö, F. Calviño, L. Canete, G. Cortès, C. Domingo-Pardo, *et al.*, Phys. Rev. C **98**, 034310 (2018).
- [53] K. Aleklett, P. Hoff, E. Lund, and G. Rudstam, Z. Phys. A **295**, 331 (1980).
- [54] T. Y. Hirsh, N. Paul, M. Burkey, A. Aprahamian, F. Buchinger, S. Caldwell, J. A. Clark, A. F. Levand, L. L. Ying, S. T. Marley, *et al.*, Nucl. Instrum. Methods Phys. Res. B **376**, 229 (2016).
- [55] G. Savard, A. F. Levand, and B. J. Zabransky, Nucl. Instrum. Methods Phys. Res. B **376**, 246 (2016).